Philosophical Magazine

ISSN: 1478-6435 (Print) 1478-6443 (Online) Journal homepage: http://www.tandfonline.com/loi/tphm20

Development of an interatomic potential for the Ni-Al system

G.P. Purja Pun & Y. Mishin

To cite this article: G.P. Purja Pun & Y. Mishin (2009) Development of an interatomic potential for the Ni-Al system, Philosophical Magazine, 89:34-36, 3245-3267, DOI: 10.1080/14786430903258184

To link to this article: http://dx.doi.org/10.1080/14786430903258184

Published online: 01 Dec 2009.

Philosophical Magazine
Vol. 89, Nos. 34–36, 1–21 December 2009, 3245–3267

Taylor & Francis
Taylor & Francis Group

Development of an interatomic potential for the Ni-Al system

G.P. Purja Pun and Y. Mishin*

Department of Physics and Astronomy, George Mason University, MSN 3F3, 4400 University Drive, Fairfax, VA 22030-4444, USA

(*Received 1 June 2009; final version received 12 August 2009*)

We construct an interatomic potential for the Ni-Al system within the embedded-atom method formalism. The potential is based on previously developed accurate potentials for pure Ni and Al. The cross-interactions are fitted to experimental cohesive energy, lattice parameter and elastic constants of B2-NiAl, as well as to *ab initio* formation energies of several real or imaginary intermetallic compounds with different crystal structures and chemical compositions. The potential accurately reproduces a variety of physical properties of the NiAl and Ni_3Al phases, and shows reasonable agreement with experimental and *ab initio* data for phase stability across the Ni-Al phase diagram. Most of the properties reproduced by the new potential were not involved in the fitting process, which demonstrates its excellent transferability. Advantages and certain weaknesses of the new potential in comparison with other existing potentials are discussed in detail. The potential is expected to be especially suitable for simulations of heterophase interfaces and mechanical behavior of Ni-Al alloys.

Keywords: atomistic simulations; interatomic potential; Ni-Al system; phase stability; interfaces; point defects

1. Introduction

Atomic-level computer simulations offer a powerful tool for gaining fundamental knowledge of materials processes and properties [1,2]. Many simulations involve large ensembles of atoms or require statistical averaging over multiple atomic events. Examples include dislocation motion, crack propagation, multicomponent diffusion, melting, crystallization and many other processes. Due to computational limitations, such large-scale simulations are presently far beyond the capabilities of first-principles (*ab initio*) methods. They are afforded by the use of semi-empirical interatomic potentials, which parameterize the configuration space of the material and express its energy as a relatively simple function of the configuration point. The energy calculations become very fast and have an order-N scaling with the number of atoms N. The potential functions depend on adjustable parameters, which are fitted to give desired properties of the material known from experiment or computed by *ab initio* methods. The basic assumption underlying this approach is that a potential fit to energies or forces for a certain set of configuration points will also give

*Corresponding author. Email: ymishin@gmu.edu

ISSN 1478–6435 print/ISSN 1478–6443 online

DOI: 10.1080/14786430903258184
http://www.informaworld.com

reasonable results for configurations between and beyond those points. This property of potentials is called 'transferability' and is the most important measure of their quality.

For metallic systems, the most common potential forms are those of the Finnis–Sinclair method [3] and the embedded atom method (EAM) [4]. In both methods, the total energy U has the form

$$U = \frac{1}{2} \sum_{i,j\,(j\neq i)} V_{s_i s_j}(r_{ij}) + \sum_i F_{s_i}(\bar{\rho}_i), \tag{1}$$

where the first term is the sum of pair interactions $V_{s_i sj}(r_{ij})$ between atom i and j with chemical species s_i and s_j. The second term is the sum of embedding energies F_{s_i} of atoms i into the host electron density $\bar{\rho}_i$ induced by all other atoms. In EAM, the host electron density is given by the sum of contributions $\rho_{s_j}(r)$ from all neighboring atoms j,

$$\bar{\rho}_i = \sum_{j\neq i} \rho_{s_j}(r_{ij}). \tag{2}$$

In the Finnis–Sinclair formalism, $\bar{\rho}_i$ is represented by a sum of pairwise functions $\Phi_{s_i s_j}(r_{ij})$, whereas $F_{s_i}(\bar{\rho}_i)$ is taken as a negative of the square root of $\bar{\rho}_i$. Although originally derived from different physical approximations (density-functional theory [4,5] or second-moment tight-binding [3]), the EAM and Finnis–Sinclair potential forms are formally similar.

Over the past 25 years, EAM and Finnis–Sinclair potentials have been applied for atomistic simulations of interfaces, dislocations, fracture, diffusion, phase transformations, deposition and many other processes. These potential forms have been proved to be capable of giving very reasonable values of elastic moduli, phonon dispersion relations, thermal expansion, melting properties, stacking fault energies, point-defect formation and migration energies, surface and interface energies and many other properties of metallic materials. For binary systems, simple phase diagrams can be reproduced in semi-quantitative agreement with experiment [6,7].

Early EAM and Finnis–Sinclair potentials were developed by fitting to a few experimental numbers. The current trend is to include a significant amount of *ab initio* information [6–16], essentially turning potentials into parameterizations of *ab initio* calculations. *Ab initio* data drastically improve the reliability of potentials by sampling large areas of configuration space, including configurations far away from areas sampled by experimental data. The *ab initio* information can be included in the form of energies or forces for real or artificial crystal structures, or forces in snapshots drawn from *ab initio* MD simulations [8]. There has been significant progress in improving the potential fitting methods [9,17,18], including approaches based on neural networks [19,20] and genetic algorithms [21,22]. Although the development of accurate and reliable potentials remains similar to art [23], new algorithms and rigorous statistical methods begin to play an increasingly important role.

In this paper, we propose a new potential for the Ni-Al system based on the EAM formalism. Several potentials have been developed for this system in the past, including the Finnis–Sinclair potential of Yan et al. [24] and the EAM potentials by

Foiles and Daw [25], Voter and Chen [26], Ludwig and Gumbsch [27] and one of the present authors [6,11]. However, most of these potentials were developed for one particular phase, either NiAl or Ni_3Al, and do not give accurate results (if tested at all) when applied to other phases of the Ni-Al system. Although the most recent potentials [6,11] have a significant degree of transferability, they leave room for further improvements.

Indeed, the potential developed in [11], which we will call EAM-2002, has a strong focus on the B2-NiAl phase. It accurately reproduces many properties on this phase, including the formation of structural Ni vacancies on the Al side of the stoichiometry. But this potential is less accurate for Ni_3Al and even less accurate for other phases. Furthermore, the pure Ni and Al functions were fitted as part of the development of the binary potential, and because the main focus was on NiAl, these functions are not intended for simulations of pure Ni or Al. On the other hand, the potential proposed in [6], which will be referred to as the EAM-2004 potential, was based on accurate Ni and Al potentials and the focus was shifted to Ni_3Al. Again, the potential reproduces many properties of Ni_3Al in good agreement with experiment and *ab initio* data. The Ni-rich part of the phase diagram was computed with this potential and was found to be in reasonable agreement with experiment [6]. However, the elastic constants and other properties of B2-NiAl predicted by this potential are not accurate.

The goal of developing yet another Ni-Al potential is two-fold. First, this is an attempt to create a more 'universal' potential for this system that would be equally accurate for NiAl, Ni_3Al, as well as pure Ni and Al. Second, this gives us an opportunity to further explore the limits of accuracy and transferability achievable by semi-empirical potentials for binary systems. In Section 2 of this paper, we describe the potential development methodology, followed by its testing for properties of NiAl (Section 3) and Ni_3Al (Section 4). Through the testing process, we compare the properties calculated with the new potential with experimental data, *ab initio* results, and predictions of the EAM-2002 and EAM-2004 potentials. In Sections 5 and 6, we discuss the transferability of the new potential to different structures, chemical compositions and temperatures. Our conclusions will be summarized in Section 7.

2. Potential development

The potential was constructed based on existing functions for pure Ni [6] and pure Al [9]. Properties of Ni and Al predicted by these two potentials have been reported in detail [6,9] and will not be repeated here. Note that the EAM-2004 potential [6] was based on the same Ni but a different Al potential. In this work, we chose a better established Al potential [9] which was used in many previous studies of mechanical behavior of this metal.

Only the cross-interaction function $V_{\mathrm{NiAl}}(r)$ was fitted in this work. It was postulated as the following combination of the existing elemental pair-interaction functions $V_{\mathrm{NiNi}}(r)$ and $V_{\mathrm{AlAl}}(r)$:

$$V_{\mathrm{NiAl}}(r) = \psi\left(\frac{r - r_c}{h}\right)\left[a_1 e^{-b_1 r} V_{\mathrm{NiNi}}(c_1(r - r_1)) + a_2 e^{-b_2 r} V_{\mathrm{AlAl}}(c_2(r - r_2))\right], \qquad (3)$$

where $\psi(x)$ is a cutoff function defined as

$$\psi(x) = \begin{cases} \dfrac{x^4}{1+x^4} & x < 0 \\ 0 & x \geq 0. \end{cases} \tag{4}$$

This function guarantees that $V_{\mathrm{NiAl}}(r)$ turns smoothly to zero at a cutoff distance r_c. Equation (3) contains 10 fitting parameters a_1, a_2, b_1, b_2, c_1, c_2,r_1, r_2, r_c and h. In addition, the potential functions were subject to the transformations

$$\rho_{\mathrm{Al}}(r) \longrightarrow s_{\mathrm{Al}}\rho_{\mathrm{Al}}(r), \tag{5}$$

$$F_{\mathrm{Al}}(\overline{\rho}) \longrightarrow F_{\mathrm{Al}}(\overline{\rho}/s_{\mathrm{Al}}), \tag{6}$$

$$F_{\mathrm{Ni}}(\overline{\rho}) \longrightarrow F_{\mathrm{Ni}}(\overline{\rho}) + g_{\mathrm{Ni}}\overline{\rho}, \tag{7}$$

$$F_{\mathrm{Al}}(\overline{\rho}) \longrightarrow F_{\mathrm{Al}}(\overline{\rho}) + g_{\mathrm{Al}}\overline{\rho}, \tag{8}$$

$$V_{\mathrm{NiNi}}(r) \longrightarrow V_{\mathrm{NiNi}}(r) - 2g_{\mathrm{Ni}}\rho_{\mathrm{Ni}}(r), \tag{9}$$

$$V_{\mathrm{AlAl}}(r) \longrightarrow V_{\mathrm{AlAl}}(r) - 2g_{\mathrm{Al}}\rho_{\mathrm{Al}}(r). \tag{10}$$

These transformations do not alter any properties of pure Ni or Al but change the shape of the cross-interaction function during the fitting process [26]. The transformation coefficients s_{Al}, g_{Ni} and g_{Al} were used as additional fitting parameters, bringing the total number of parameters to 13.

The fitting database included the experimental values of the lattice parameter a_0, formation energy E_f and elastic constants c_{ij} of the B2 structure of NiAl. The *ab initio* part of the database included the formation energies E_f of the following nine ordered structures of the Ni-Al system: $L1_2$-Ni_3Al, $D0_{22}$-Ni_3Al, $D0_3$-Ni_3Al, B1-NiAl, $L1_0$-NiAl, $L1_1$-NiAl, B32-NiAl, 40-NiAl (NbP prototype) and $L1_2$-Al_3Ni. The formation energy E_f of a compound Ni_nAl_m is defined by

$$E_f = \frac{E_0(\mathrm{Ni}_n\mathrm{Al}_m) - nE_0(\mathrm{Ni}) - mE_0(\mathrm{Al})}{n+m}, \tag{11}$$

where E_0 are cohesive energies of the respective elements or compounds. The *ab initio* data used in this work were computed in [11]. Note that by contrast to the previous potentials [6,11] where energy-volume relations of the structures were included in the fit, in this work we used only the minimum-energy values obtained from such relations. Thus, the potential was not 'informed' about the equilibrium lattice parameters or bulk moduli of those nine structures. The smaller database used in this work was commensurate with the smaller number of fitting parameters in comparison with the previous potentials [6,11].

The potential function (3) was optimized by minimizing the weighted mean-squared deviation of properties from their target values using the simulated annealing method. Figure 1 shows the obtained potential functions in the effective-pair format [28]. Tabulated forms of the potential functions are available for download from http://www.ctcms.nist.gov/potentials/ or from the authors by request.

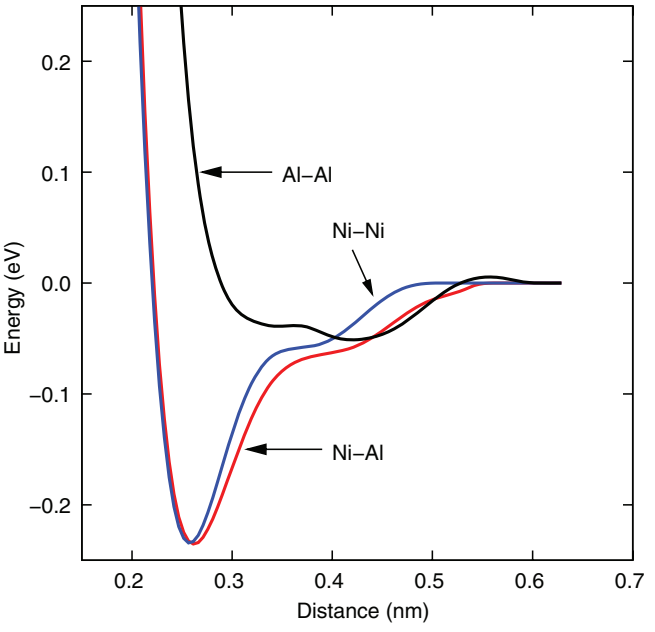

Figure 1. Pair-interaction functions of the new EAM potential presented in the effective pair format.

3. Properties of B2-NiAl

3.1. *Lattice properties and structural stability*

The potential reproduces the lattice parameter, cohesive energy and elastic constants of B2-NiAl in good agreement with experiment and on the level of accuracy of the EAM-2002 potential (Table 1). These properties were included in the potential fit.

The phonon dispersion curves computed with the new potential are shown in Figure 2. The agreement with experiment (inelastic neutron scattering at room temperature) is very good at low frequencies, with a trend to overestimate the frequencies of optical phonons. The EAM-2002 potential was also accurate at low frequencies but the discrepancy at high frequencies was larger than with the new potential.

Thermal expansion factors of NiAl were computed by NPT Monte Carlo simulations and were found to be in excellent agreement with experiment at all temperatures 293 K to the melting point (Figure 3). In fact, the agreement is significantly better than with the EAM-2002 potential, even though the latter was fit to thermal expansion factors while the new potential was not. The deviations from the experimental data at low temperatures are due to the quantum effects in vibrations, which are not captured by the classical Monte Carlo method.

Table 2 summarizes the formation energies of NiAl compounds with different crystalline structures. The new potential is in significantly better agreement with *ab initio* calculations than the previous potentials [6,11]. This improved agreement with respect to phase stability is important for asserting the transferability of the potential.

Table 1. Lattice properties of B2-NiAl calculated with the new EAM potential in comparison with the EAM-2002 potential [11] and experimental data. These properties were included in the potential fit.

	Experiment	EAM (present)	EAM-2002[†]
a_0 (Å)	2.88[a]	2.83	2.86
E_0 (eV)	−4.50[b]	−4.51	−4.47
c_{11} (GPa)	199[c]	191	200
c_{12} (GPa)	137[c]	143	140
c_{44} (GPa)	116[c]	121	120

[†]Ref. [11]; [a]Ref. [68]; [b]Ref. [69]; [c]Ref. [70].

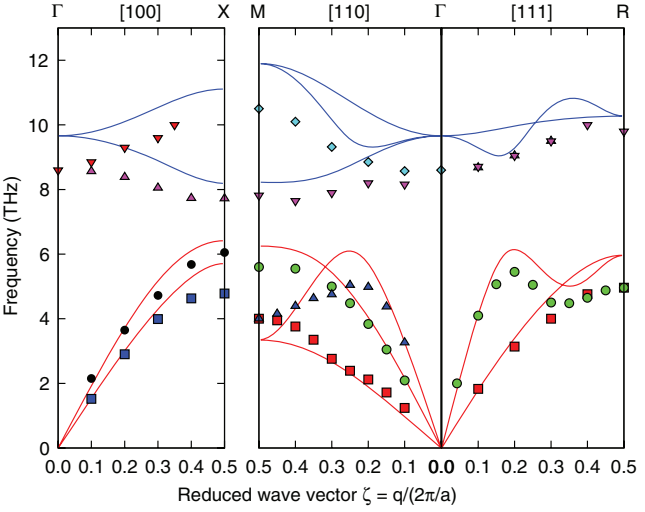

Figure 2. Phonon dispersion relations in B2-NiAl calculated with the new EAM potential (lines) in comparison with experimental data (points) [81].

To further evaluate the transferability of the potential to regions of configuration space that are far away from equilibrium, energy along two homogeneous deformation paths was computed and compared with *ab initio* calculations. For the Bain deformation path (Figure 4), the initially equilibrium B2 structure was elongated or compressed along a [001] direction with a simultaneous compression or elongation in two other cubic directions to preserve the atomic volume. When the tetragonal distortion c/a reaches $\sqrt{2}$, the B2 structure transforms into ideal $L1_0$ structure. Figure 4 demonstrates that the new potential is in slightly better agreement with *ab initio* results than the EAM-2002 potential under compression but is slightly less accurate under tension. Overall, however, both potential are in good agreement with *an initio* calculations. Note that the $L1_0$ structure does not produce any energy minimum, indicating its instability with respect to tetragonal distortions at this atomic volume. Calculations show that even if the volume is allowed to vary, the $L1_0$ structure is still mechanically unstable.

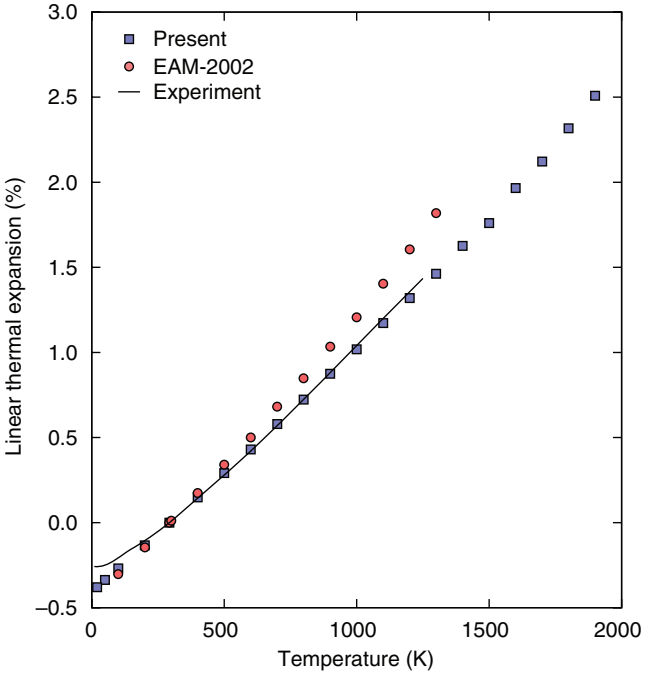

Figure 3. Linear thermal expansion (%) of B2-NiAl relative to room temperature (293 K) computed with the new EAM potential in comparison with the EAM-2002 potential [11] and experimental data [82].

Table 2. Formation energies of selected crystal structures of the NiAl and Ni_3Al compounds calculated with the new EAM potential in comparison with the EAM-2002 [11] and EAM-2004 [6] potentials and with *ab initio* (LAPW) results [11] when available. The structures marked by an asterisk were not included in the fit of the new potential. The numbers typeset in bold are in closest agreement with *ab initio* data.

Phase	Structure	*Ab initio*	EAM	EAM-2002	EAM-2004
Ni_3Al	$L1_2$	−0.4680	**−0.4540**	−0.3837	−0.4486
	$D0_{22}$	−0.4305	−0.4474	−0.3745	**−0.4318**
	$D0_3$	−0.4093	**−0.4213**	−0.3245	−0.4356
	$D0_{11*}$		−0.0827	−0.0464	−0.0147
	$D0_{23*}$		−0.4520	−0.3793	−0.4401
	$D0_{19*}$		−0.4503	−0.3681	−0.4392
NiAl	B2	−0.7041	**−0.6059**	−0.5337	−0.5918
	B1	−0.0335	**−0.0337**	−0.0564	−0.0596
	$L1_0$	−0.5469	−0.4811	−0.3615	**−0.5139**
	$L1_1$	−0.3251	**−0.3343**	−0.1509	−0.3590
	B32	−0.3544	**−0.3736**	−0.1634	−0.4721
	'40'(NbP)	−0.5435	−0.4728	−0.3368	**−0.4762**
	B20*		−0.4901	−0.4035	−0.4283

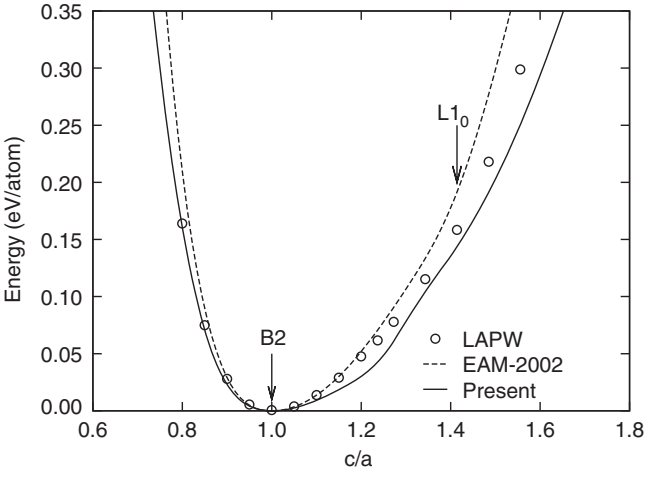

Figure 4. Energy along the volume-conserving Bain path of B2-NiAl computed with the new EAM potential in comparison with the EAM-2002 potential [11] and *ab initio* (LAPW) calculations [11]. The energies are given relative to the equilibrium B2-NiAl phase.

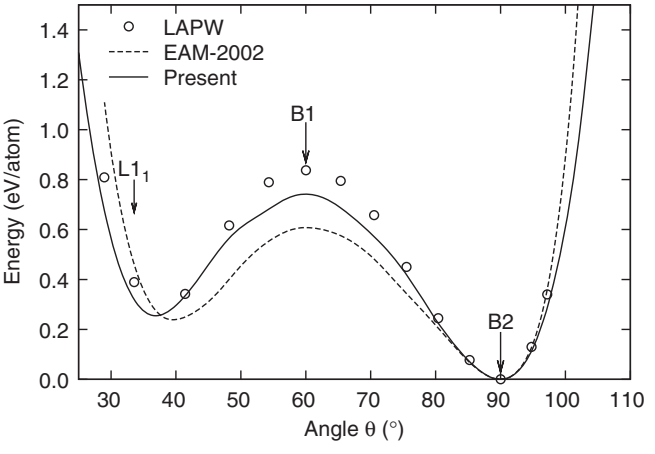

Figure 5. Energy along the volume-conserving trigonal deformation path of B2-NiAl computed with the new EAM potential in comparison with the EAM-2002 potential [11] and *ab initio* (LAPW) calculations [11]. θ is the angle between the initial $\langle 100 \rangle$ directions in the B2 structure. This angle is varied to obtain the B1 and $L1_1$ structures. The energies are given relative to the equilibrium B2-NiAl phase.

For the trigonal deformation path (Figure 5), the B2 structure was stretched along the [111] direction and simultaneously compressed in normal directions to preserve the volume. The degree of the trigonal distortion is characterized by the angle θ between the lattice translation vectors with $\theta = 90^\circ$ for the B2 structure. The angles $\theta = 60^\circ$ and $\theta = 33.6^\circ$ produce the B1 and $L1_1$ structures, respectively. The new potential demonstrates a significant improvement of the agreement with *ab initio* data in comparison with the EAM-2002 potential. We emphasize that this

Table 3. Surface, antiphase boundary (APB) and unstable stacking fault energies ($J\,m^{-2}$) in B2-NiAl calculated with the new EAM potential in comparison with the EAM-2002 potential [11], experimental and *ab initio* data. The (100) and (111) surface energies represent average values over the Ni and Al terminations. These properties were not included in the potential fit.

	Experiment	*Ab initio*	EAM (present)	EAM-2002[†]
Surface				
(100)		2.85[a], 2.75[b]	2.12	1.67
(110)		2.05[b], 1.87[c], 1.79[d], 1.37[d]	1.89	1.25
(111)			2.20	1.63
APB				
(110)	>0.50[e]	0.88[f], 0.81[g]	0.65	0.55
(211)	>0.75[e]	0.89[f], 0.99[g]	0.73	0.72
Unstable fault				
(100)⟨001⟩		1.3[a], 3.35[h]	1.56	1.24
(110)⟨001⟩		2.85[h]	1.12	0.83

[†]Ref. [11]; [a]Ref. [71]; [b]Ref. [72]; [c]Ref. [73]; [d]Ref. [70]; [e]Ref. [31]; [f]Ref. [32]; [g]Ref. [33]; [h]Unrelaxed energy, Ref. [36].

better agreement resulted without any fitting, pointing to an improved transferability of the potential.

3.2. *Surfaces and stacking faults*

The EAM-2002 potential tended to underestimate the surface energies of B2-NiAl (Table 3). As indicated in Table 3, the new potential predicts significantly higher surface energies, which are in a much better agreement with *ab initio* calculations. Again, this improvement was achieved without any fitting. The improved surface energies are important because they make the potential more suitable for simulations of fracture, ensuring the correct balance between the energies of the newly formed surfaces and the unstable stacking fault energy [29].

To assess the suitability of the potential for simulations of plastic deformation of NiAl, γ-surfaces on different crystal planes were calculated. The γ-surface is a plot of a generalized stacking fault energy γ as a function of displacement along different directions in the fault plane [30]. The fault energy is calculated by minimizing the total energy with respect to atomic displacements in the direction normal to the fault plane while prohibiting displacements in parallel directions. Minima and maxima of the γ-surface correspond to stable and unstable planar faults. Vectors connecting energy minima give Burgers vectors of possible dislocations, while the unstable stacking fault energies give the barriers for the formation of stable faults. Thus, γ-surfaces are useful for predicting possible dislocation reactions, core dissociations and other properties relevant to mechanical behavior.

Figure 6 shows [111] sections of γ-surfaces on the (110) and (211) planes of B2-NiAl. The minimum on each curve corresponds to the formation of a stable antiphase boundary (APB) on the respective crystal plane. From these plots, it can be predicted that a perfect [111] dislocation will dissociate into 1/2[111] superpartials separated by an APB on the (110) or (211) plane. In reality, the APB energies are so

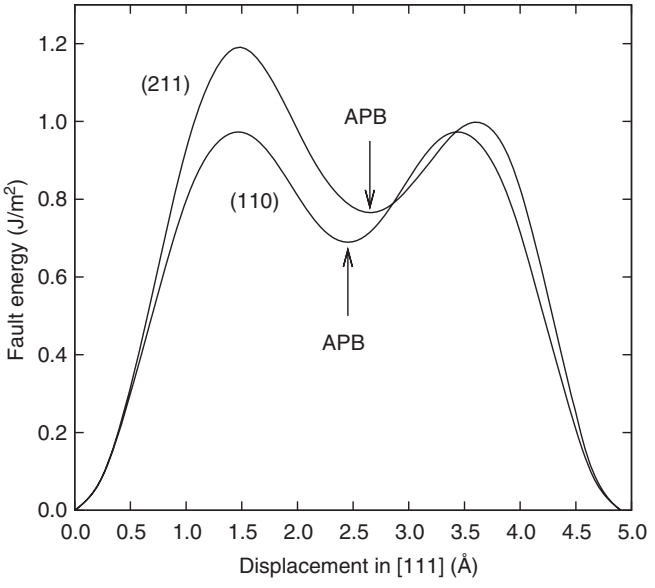

Figure 6. Sections of γ-surfaces of B2-NiAl on the (110) and (211) planes in the [111] direction computed with the new EAM potential. The energy minima shown by arrows correspond to antiphase boundaries (APB).

large that the core splitting is beyond the resolution of transmission electron microscopy. From this experimental fact, the lower bounds of the APB energies were estimated to be $0.5\,\mathrm{J\,m^{-2}}$ for the (110) plane and $0.75\,\mathrm{J\,m^{-2}}$ for the (211) plane [31]. *Ab initio* calculations [32,33] give value consistent with these bounds (Table 3). Both the new and the EAM-2002 potentials predict (110) APB energies above the experimental lower bound but below the *ab initio* calculations, with the new potential being in a better agreement with the *ab initio* results. For the (211) APB, both potentials give energies close to the experimental lower bound but significantly below the *ab initio* calculations. It should be noted that the APB energies listed in Table 3 are fully relaxed and thus slightly lower than the values on the γ-surfaces. We also emphasize that the (110) APB energy was included in the fitting of the EAM-2002 potential but not in the fitting of the new potential. The (211) APB energy was not in the fit for either potential.

Considering that the preferred slip in NiAl is with the Burgers vector [001] [34], we have also computed [001] cross-sections of γ-surfaces on (100) and (110) planes (Figure 7). The single energy maximum observed in both cross-sections indicates that the [001] dislocation should have a compact core, which is consistent with transmission electron microscopy observations [35]. The height of the energy maximum represents the unstable stacking fault energy, whose values for the (100) and (110) planes are given in Table 3. Both potentials are in agreement with *ab initio* data (note that the fault energies reported in [36] are unrelaxed and should be considered as upper bounds of the true energies) and are consistent with the easiest slip on the (110)[001] system observed experimentally [34].

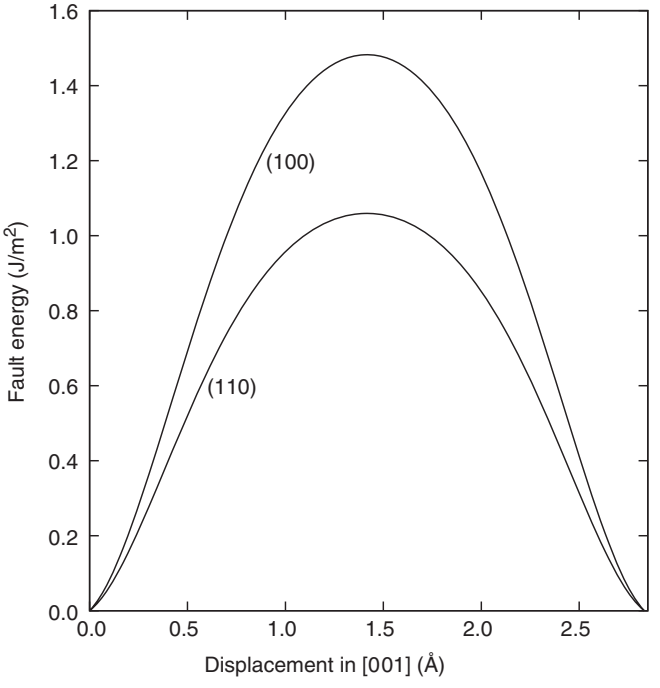

Figure 7. Sections of γ-surfaces of B2-NiAl on the (100) and (110) planes in the [001] direction computed with the new EAM potential. The energy maxima give the unstable stacking fault energies.

3.3. *Point defects*

The new potential has been tested for point-defect properties of B2-NiAl. The results are compared with *ab initio* data in Table 4. Before making conclusions from this comparison, an explanation should be given of the quantities appearing in this table.

The B2-NiAl compound contains two sublattices and supports four types of point defects: vacancies on the Ni and Al sublattices (V_{Ni} and V_{Al}) and antisite defects Al_{Ni} (Al atom on the Ni sublattice) and Ni_{Al} (Ni atom on the Al sublattice). These defects can have a strong impact on thermodynamic properties and diffusion in this compound, especially near the stoichiometric composition. Furthermore, B2-NiAl displays the so-called triple-defect mechanism of compositional disorder, in which derivations from the exact stoichiometry on the Al-rich side are accommodated predominantly by vacancies on the Ni sublattice, whereas on the Ni-rich side they are accommodated by antisite defects on the Al sublattice (Ni_{Al}). The majority of other intermetallic compounds form antisites on both sides of the stoichiometry. The triple-defect mechanism of compositional disorder observed in B2-NiAl has been verified both experimentally [37,38] and by *ab initio* calculations [39–41], and it was built into the development of the EAM-2002 potential.

The condition that Al-rich compositions on B2-NiAl favor the formation of Ni structural vacancies over Al_{Ni} antisites can be formulated as a certain relation between point-defect energies. Specifically, the so-called interbranch-Al energy [39],

Table 4. Energies (in eV) of composition-conserving point-defect complexes in B2-NiAl calculated with the new EAM potential in comparison with the EAM-2002 potential [11] and *ab initio* data. ε_d denotes the 'raw' formation energy of defect d. All other notations are explained in the text. These energies were not included in the potential fit.

Complex	Equation	*Ab initio*	EAM (present)	EAM-2002[†]
Exchange	$\varepsilon_{Ni_{Al}} + \varepsilon_{Al_{Ni}}$	3.15[a], 3.10[b], 3.63[c], 2.65[d]	2.075	2.765
Divacancy	$\varepsilon_{V_{Ni}} + \varepsilon_{V_{Al}} + 2E_0$	3.07[a], 2.71[b], 2.53[c], 2.18[d]	2.569	2.396
Triple-Ni	$2\varepsilon_{V_{Ni}} + \varepsilon_{Ni_{Al}} + 2E_0$	2.83[a], 2.22[b], 2.36[c], 1.58[d]	2.807	2.281
Triple-Al	$2\varepsilon_{V_{Al}} + \varepsilon_{Al_{Ni}} + 2E_0$	6.46[a], 6.30[b], 6.32[c], 5.44[d]	4.406	5.276
Interbranch-Ni	$2\varepsilon_{V_{Al}} - \varepsilon_{Ni_{Al}} + 2E_0$	3.31[a], 3.20[b], 2.69[c], 2.78[d]	2.331	2.511
Interbranch-Al	$\varepsilon_{Al_{Ni}} - 2\varepsilon_{V_{Ni}} - 2E_0$	0.32[a], 0.88[b], 1.28[c], 1.07[d]	−0.732	0.484

[†]Ref. [11]; [a]Ref. [42]; [b]Ref. [43]; [c]Ref. [39]; [d]Ref. [41].

that will be defined below, must be positive. This energy at zero Kelvin predicted by *ab initio* calculations [39,41–43] ranges widely from 0.32 eV [42] to as high as 1.28 eV [39], depending on computational details. During the development of the EAM-2002 potential [11], a positive value of the interbranch-Al energy was enforced. The value actually achieved by the fit was 0.48 eV, which compares well with *ab initio* predictions.

It should be pointed out that point-defect calculations in ordered compounds are not as straightforward as in elemental solids. One can readily calculate the so-called 'raw' formation energy of a defect, which is defined as the energy difference between a simulation block with a single point defect and the same block without any defects [44,45]. However, this difference depends on reference constants involved in the energy calculations. 'Raw' energies of point defects can have very different values in *ab initio*, EAM and other calculation methods. Since the equilibrium point defect concentrations are independent of any reference constants, they can only depend on such combinations of 'raw' energies in which the reference constants cancel out. To meet this requirement, it was proposed to express point defect concentrations through formation energies of so-called composition-conserving defect complexes [39,41,46]. Such complexes can be considered as thermal excitations that automatically preserve the chemical composition. It can be shown [39,41,46] that the knowledge of formation energies of any three of such complexes is sufficient for computing all point defect concentrations.

Examples of composition-conserving defect complexes include the interbranch-Al defect which creates an antisite on the Ni sublattice instead of two Ni vacancies ($Al_{Ni} - 2V_{Ni}$), and the interbranch-Ni defect which creates two Al vacancies and eliminates an antisite on the Al sublattice ($2V_{Al} - Ni_{Al}$). Expressions for the energies of these and other complexes in terms of 'raw' energies of individual point defects are given in Table 4. Since the complex energies are independent of reference constants, they are suitable for comparing calculations performed by different methods. Table 4 compares predictions of the new potential with *ab initio* results and calculations with the EAM-2002 potential. The important observation is that the new potential unfortunately gives a negative interbranch-Al energy, which is in disagreement with the predominance of Ni structural vacancies in Al-rich compositions. For all other energies, both potentials are in about the same good agreement with *ab initio* calculations.

Table 5. Lattice properties of Ni_3Al predicted by the new EAM potential in comparison with the EAM-2004 potential [6] and experimental data. Only the cohesive energy E_0 was included in the potential fit.

	Experiment[a]	EAM (present)	EAM-2004[†]
a_0 (Å)	3.57	3.533	3.571
E_0 (eV)	−4.620	−4.631	−4.626
c_{11} (GPa)	230	238	236
c_{12} (GPa)	149	166	154
c_{44} (GPa)	132	130	127

[a]Ref. [74,75]; [†]Ref. [6].

4. Properties of $L1_2$-Ni_3Al

Testing the potential for Ni_3Al properties was especially important because the only quantity related to this compound that was included in the potential fit was its formation energy. Thus, all comparisons between predictions of this potential and available experimental or *ab initio* data are essentially tests of its transferability.

4.1. *Lattice properties*

Table 5 demonstrates that the lattice parameter and elastic constants of Ni_3Al predicted by the new potential are in about the same good agreement with experimental data as the EAM-2004 potential. The latter, however, was directly fitted to these properties, whereas the new potential was not.

The phonon dispersion relations computed at 0 K are in reasonable agreement with experimental results obtained by inelastic neutron scattering at room temperature [47]. The acoustic branches are reproduced with excellent accuracy, whereas the frequencies of the upper optical branches are somewhat overestimated. Nevertheless, even in the high-frequency range, the agreement with experiment is better than with the EAM-2004 potential [6]. We emphasize that neither of the two potentials was fitted to phonon frequencies.

The thermal expansion factors computed by NPT Monte Carlo simulations are in fair agreement with experimental data but are less accurate than with the EAM-2004 potential (Figure 8). The discrepancies at low temperatures are caused by quantum effects which are not included in the Monte Carlo method.

The formation energies of several different compounds with the same Ni_3Al stoichiometry are listed in Table 2. The new potential is in significantly better agreement with *ab initio* calculations than the EAM-2002 potential and in slightly better agreement than the EAM-2004 potential. Note, however, that the ordering of the energies of the different structures is the same for all three potentials and matches the *ab initio* energies with only one exception: the EAM-2004 potential predicts the $D0_{22}$ structure to be slightly (0.004 eV) more stable than $D0_3$, which is in disagreement with *ab initio* data.

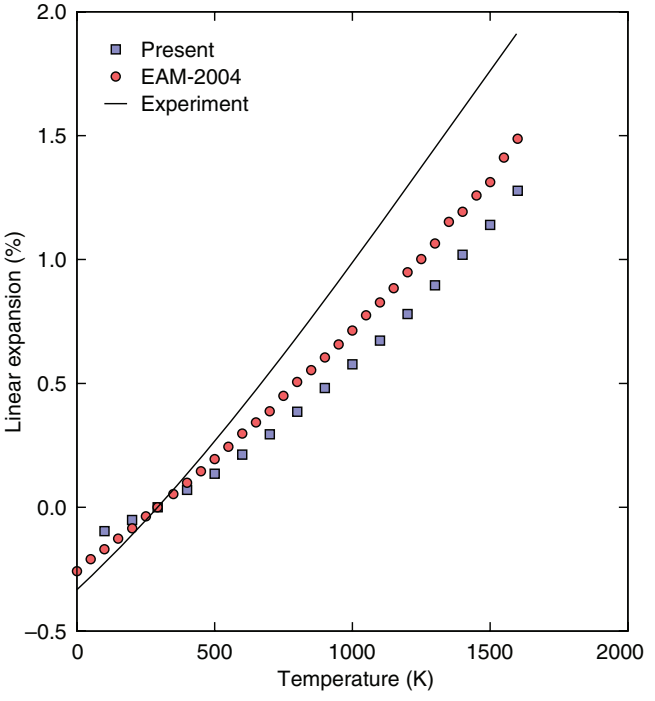

Figure 8. Linear thermal expansion (%) of Ni_3Al relative to room temperature (293 K) computed with the new EAM potential in comparison with the EAM-2004 potential [11] and experimental data [82].

Table 6. Calculated and experimental energies (in $mJ\,m^{-2}$) of surfaces and planar faults in Ni_3Al predicted by the new EAM potential in comparison with the EAM-2004 potential [6], *ab initio* and experimental data. These properties were not included in the potential fit.

	Experiment	*Ab initio*	EAM (present)	EAM-2004[†]
Surface				
(100)			2150	1711
(110)			2257	1847
(111)			1966	1483
Planar fault				
APB(111)	180[a], 175[b], 195[c]	188[d], 210[e], 172[f]	249	252
CSF(111)	206[a], 235[b], 236[c]	225[e], 223[f]	193	202
SISF(111)	6[b]	80[e], 79[f]	37	51
APB(100)	104[b], 160[c]	121[g]	74	80

[†]Ref. [6]; [a]Ref. [56]; [b]Ref. [57]; [c]Ref. [58]; [d]Ref. [52]; [e]Ref. [53]; [f]Ref. [54]; [g]Ref. [55].

4.2. *Planar defects*

The energies of low-index surfaces of Ni_3Al are given in Table 6. We are not aware of any reliable experimental or *ab initio* data that could be used for comparison. However, it is known that EAM potentials tend to underestimate surface energies of

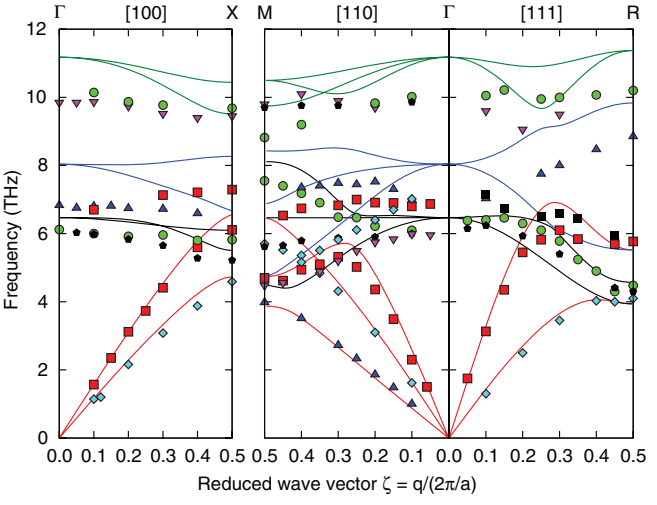

Figure 9. Phonon dispersion relations in Ni_3Al calculated with the new EAM potential (lines) in comparison with experimental data (points) [47].

metals and intermetallic compounds [28]. The fact that the surface energies predicted by the new potential are significantly higher than those predicted by the EAM-2004 potential may suggest that the new potential represents surface energies more accurately. This conjecture will need to be tested by future calculations or measurements.

For simulations of mechanical behavior of Ni_3Al, it is important for the potential to reproduce the energies of stacking faults on (111) and (001) crystal planes. Indeed, plastic deformation of this compound is influenced by the core structure of ⟨110⟩ screw superdislocations. These dislocations can dissociate into superpartials by one of two different schemes. In one, the dislocation dissociates into $1/2\langle 110\rangle$ superpartials separated by an APB on a (111) plane [48–51]. Each of the superpartials can dissociate into Shockley partials bounding a complex stacking fault (CSF). Alternatively, the dislocation can dissociate into $1/3\langle 211\rangle$ Kear superpartials bounding a superlattice intrinsic stacking fault (SISF). Thus, the dislocation core structure and mobility depend on the energies of three planar faults on the (111) plane: APB, CSF and SISF. At high temperatures, the leading superpartial can cross-slip into a (001) plane and form a locked configuration. This lock includes a (001) APB, whose energy is assumed to be smaller than the energy of the (111) APB providing a driving force of the cross-slip. This cross-slip and the lock formation are responsible for the flow stress anomaly in Ni_3Al [48–51].

The γ-surfaces on the (111) and (001) planes were computed using the methodology as discussed in [6]. The results are summarized in Table 6 and compared with *ab initio* calculations [52–55] and experimental data obtained by transmission electron microscopy [56–58]. Both the new and the EAM-2004 potential demonstrate satisfactory agreement with experimental and *ab initio* energies without any fitting. The lower energy of the (001) APB relative to the (111) APB is consistent with the existence of driving force for the cross-slip process, although the anisotropy

of the APB energy is overestimated in comparison with both experiment and *ab initio* results. The SISF energy predicted by both potentials is between the *ab initio* and experimental values. The large gap between the *ab initio* and experimental results for the SISF energy is still a mystery; see discussion in [6].

4.3. *Point defects*

As in the case of B2-NiAl, the Ni_3Al compound supports four types of point defects: a vacancy and an antisite on each sublattice. As discussed in Section 3.3, the 'raw' energies of individual point defects depend on reference constants and are useful only as input for calculations of point-defect concentrations [6,44,45,59] from a lattice gas model [39,41–43,59]. Exact solutions of the model can be obtained only numerically, but one can derive approximate analytical solutions for some limiting cases [6,59].

According to experimental data [60] and *ab initio* calculations [61], thermal disorder in Ni_3Al is dominated by antisite defects on either side of the stoichiometry, with vacancy concentrations being orders of magnitude smaller. Using this fact, approximate analytical expressions have been derived [6] that express point-defect concentrations as Arrhenius exponentials of so-called effective formation energies. Table 7 gives expressions for the effective formation energies of point defects in stoichiometric Ni_3Al in terms of their 'raw' energies, along with results obtained with the new and EAM-2004 potentials. The new potential shows a better agreement with *ab initio* energies for the Al vacancy but is somewhat less accurate for the Ni vacancy and the antisites. Overall, however, both potentials perform equally well. In particular, the significantly higher vacancy formation energies relative to the antisite energies are consistent with the predominantly antisite disorder mechanism, justifying the approximations underlying the analytical solutions.

5. Phase stability in the Ni-Al system

Table 8 summarizes the cohesive energies and lattice constants of different phases of the Ni-Al system computed with the new potential. The results predicted by the potential compare reasonably well with experimental data when available, including phases that were not included in the potential fit.

Table 7. Effective formation energies (in eV) of point defects in Ni_3Al predicted by the new EAM potential in comparison with the EAM-2004 potential [6] and *ab initio* calculations. The notations are explained in the text. These energies were not included in the potential fit.

Defect	Equation	*Ab initio*[a]	EAM (present)	EAM-2004[†]
V_{Ni}	$\varepsilon_{V_{Ni}}+E_0+\frac{1}{8}(\varepsilon_{Ni_{Al}}-\varepsilon_{Al_{Ni}})$	1.863	1.571	1.628
V_{Al}	$\varepsilon_{V_{Al}}+E_0-\frac{3}{8}(\varepsilon_{Ni_{Al}}-\varepsilon_{Al_{Ni}})$	2.673	2.145	1.850
Al_{Ni}	$\frac{1}{2}(\varepsilon_{Ni_{Al}}+\varepsilon_{Al_{Ni}})$	0.720	0.633	0.837
Ni_{Al}	$\frac{1}{2}(\varepsilon_{Ni_{Al}}+\varepsilon_{Al_{Ni}})$	0.720	0.633	0.837

[†]Ref. [11].

Another way of comparing the potential predictions with experiment is to plot the formation energies E_f of different intermetallic compounds versus their chemical composition. The formation energies were computed from Equation (11). A convex-hull construction of this plot gives the set of structures that should be observed on the experimental phase diagram at low temperatures. The formation energies of all other structures must lie above the convex hull. Figure 10 shows this construction for the new potential. The intermetallic phases predicted to be stable are Ni_5Al_3, Ni_3Al and NiAl with the crystal structures of Ga_3Pt_5, $L1_2$ and B2, respectively. These compounds with exactly these crystal structures are indeed observed on the experimental phase diagram [62]. All other crystal structures with these stoichiometries have energies above the tie lines, as they should. Furthermore, the Ni_5Al_3 formation energy is just slightly below the line connecting Ni_3Al and NiAl, suggesting that this phase is barely stable and should form at significantly lower temperatures than other phases, which is again very consistent with the experimental

Table 8. Equilibrium lattice parameters (a_0) and cohesive energies (E_0) of selected phases of the Ni-Al system calculated with the new EAM potential in comparison with experimental data where available. For non-cubic structures, two or three lattice parameters are listed. The asterisk indicates structures which were not included in the potential fit.

		Experiment		EAM	
Phase	Structure	a_0 (Å)	E_0 (eV)	a_0 (Å)	E_0 (eV)
Ni	A1	3.52[a]	−4.45[b]	3.52	−4.45
Ni_3Al	$L1_2$	3.57[c]	−4.57[d]	3.5332	−4.6315
	$D0_{22}$			3.5329	−4.6249
	$D0_3$			5.5425	−4.5988
	$D0_{11*}$			6.0265, 7.0703, 4.4186	−4.2602
	$D0_{23*}$			3.5338	−4.6295
	$D0_{19*}$			4.9910, 4.0645	−4.6278
NiAl	B2	2.88[a]	−4.50[d]	2.8320	−4.5109
	B1			4.7535	−3.9387
	$L1_0$			3.6309	−4.3861
	$L1_1$			3.6718	−4.2393
	B32			4.9689	−4.2786
	40(NbP)			3.4685	−4.3778
	B20*			4.5815	−4.3951
Ni_3Al_4	Ni_3Ga_{4*}	11.408[e]		11.275	−4.2658
Ni_2Al_3	$D5_{19*}$	4.03, 4.88[f]	−4.38[f]	3.9970, 4.8527	−4.1580
Ni_5Al_3	Ga_3Pt_{5*}			7.4181, 6.5256, 3.7077	−4.5782
$NiAl_3$	$D0_{11*}$	6.60, 7.35, 4.80[f]	−4.02[f]	6.4622, 7.5677, 4.8661	−3.8741
	$L1_{2*}$			3.8015	−3.8931
	$D0_{3*}$			5.9891	−3.8360
	$D0_{22*}$			3.7980	−3.8900
	$D0_{23*}$			3.7994	−3.8916
	$D0_{19*}$			5.3720, 4.3517	−3.8970
Ni_2Al	$C11_{b*}$			2.8037, 8.4110	−4.5546
$NiAl_2$	$C11_{b*}$			2.9435, 8.8304	−4.1050
Al	A1	4.05[a]	−3.36[b]	4.05	−3.36

[a]Ref. [67]; [b]Ref. [75]; [c]Ref. [37,76]; [d]Ref. [77]; [e]Ref. [78]; [f]Ref. [79,37].

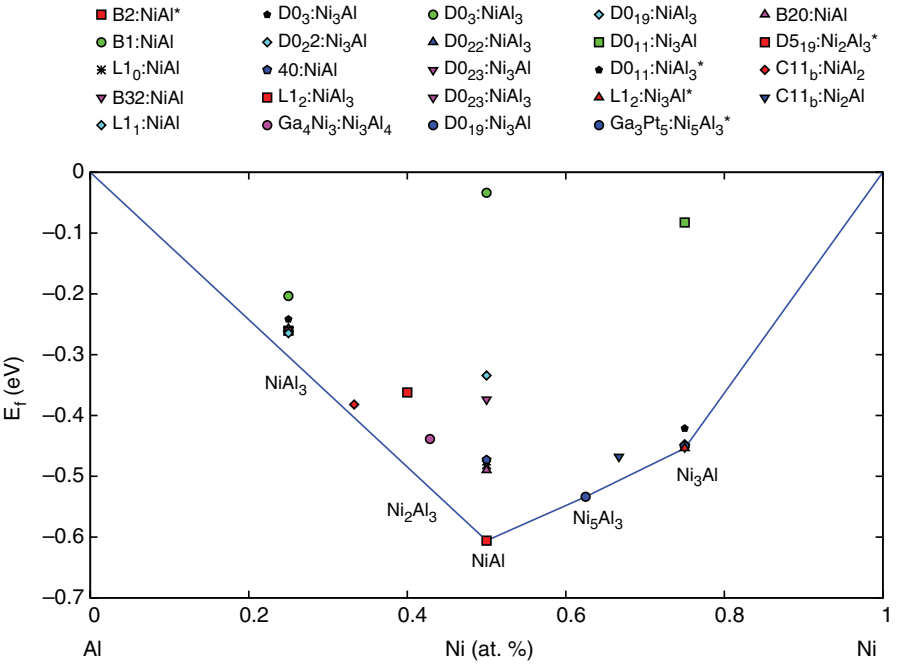

Figure 10. Formation energy of experimentally observed or imaginary intermetallic compounds of the Ni-Al system predicted by the new EAM potential. The compounds marked by an asterisk and labeled in the plot are observed on the experimental phase diagram.

phase diagram [62]. It should be noted that the EAM-2002 and EAM-2004 potentials give Ni_5Al_3 formation energies lying above the Ni_3Al-NiAl tie line, in contradiction to the experimental phase diagram.

However, the formation energies of the Ni_2Al_3 and $NiAl_3$ compounds which appear on the experimental phase diagram lie above the NiAl-Ni line, indicating that the potential underestimates their binding. In addition, the potential predicts that the energy of the $D0_{19}$ structure of $NiAl_3$ is slightly below the experimentally observed $D0_{11}$ structure, which is also incorrect. Again, the EAM-2002 and EAM-2004 potentials had similar problems in reproducing the Al-rich part of the phase diagram. It should be pointed out that this analysis of phase stability is based on 0 K energies. At finite temperatures, atomic vibrations can affect the free energies of the crystal structures and alter their relative stability. The energy differences between some of the competing structures discussed here are as small as a few meV.

6. Melting temperatures of the phases

The transferability of the potential to high temperatures was evaluated by computing the melting points of Ni, NiAl and Ni_3Al. We employed all-periodic simulation blocks consisting of solid and liquid phases separated by a (001) interface (see example for Ni_3Al in Figure 11a). The blocks contained 9 to 16 thousand

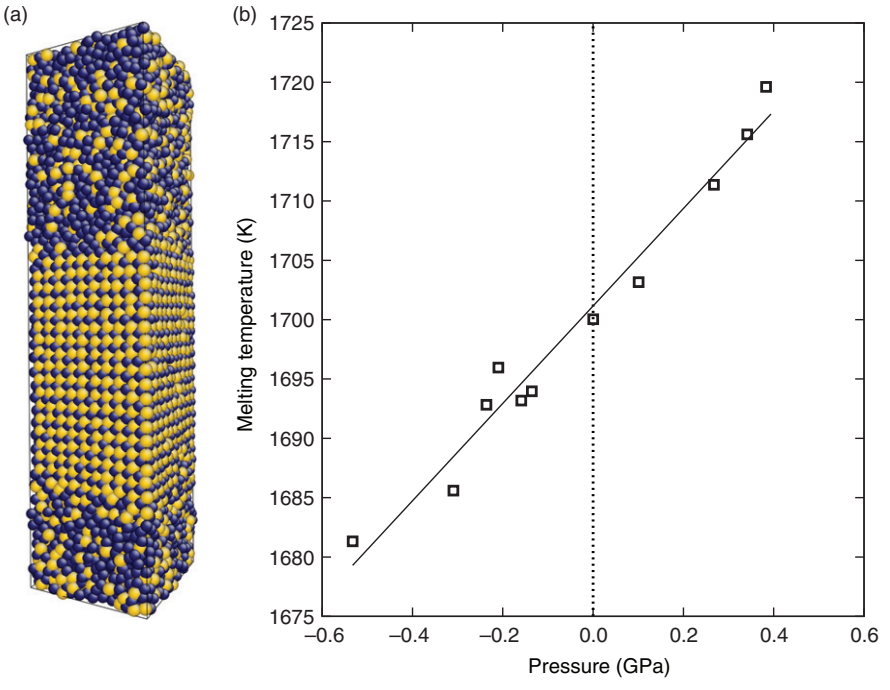

Figure 11. Examples of calculation of melting points. (a) Simulation block used for calculation of the melting temperature of Ni_3Al, with dark and bright points representing Ni and Al atoms. The solid–liquid interface orientation is (001). (b) Melting temperature versus pressure for pure Ni. The dotted vertical line corresponds to zero pressure and is shown as a guide to the eye. The linear fit (solid line) is used to calculate the melting point at zero pressure.

atoms and were 100–150 Å thick in the direction normal to the interface. The blocks were created by melting a half of an initially single-phase solid system, which in the case of NiAl and Ni_3Al had a perfectly stoichiometric chemical composition.

To calculate the melting temperature T_m, the system was first brought to mechanical equilibrium at some temperature close to the expected T_m value by an NPT MD run (fixed temperature, number of atoms and zero pressure). The MD ensemble was then switched to microcanonical (NVE) and an additional 4 ns long run was performed. During this run, some partial melting or crystallization could occur, after which the temperature and pressure leveled out at new constant values. These values were determined by averaging over the last 2 ns of the NVE run, giving a melting temperature and the corresponding pressure. Such simulations were repeated several times starting from different snapshots saved during the NPT run, producing a plot of the melting temperature versus pressure. An example of such a plot is shown in Figure 11b for pure Ni. The final value of T_m was obtained by linear interpolation to zero pressure.

Table 9 summarizes the obtained melting temperatures in comparison with experimental data.[1] The melting temperature of Al [9] calculated by the same method elsewhere [64] has been added for completeness. The melting points of Ni and Ni_3Al are in excellent agreement with experiment. The melting temperatures of NiAl and

Table 9. Melting temperatures (in K) of selected phases of the Ni-Al system calculated with the new potential in comparison with experimental data [62,63].

Phase	Ni	Ni_3Al	NiAl	Al
EAM (present)	1701	1678	1780	1042
Experiment	1728	1645	1911	933
Discrepancy (%)	1.6	1.9	6.8	11.7

especially Al are less accurate but still reasonable. The main point of this comparison, however, is that *none* of these melting temperatures or any liquid properties, in fact not even any finite-temperature properties of the phases, were included in the potential fit. It is always possible to achieve an accurate match to the experimental melting point by including it in the fitting process. That the four melting points listed in Table 9 have been *predicted* by the new potential at this level of accuracy, without *any* fit, speaks for its very good transferability to high temperatures.

7. Discussion and conclusions

The Ni-Al potential developed in this work accurately reproduces a variety of physical properties of *both* NiAl *and* Ni_3Al. In addition, it demonstrates a fairly good agreement with experimental and *ab initio* data for the formation energies of several other compounds of the Ni-Al system. The overwhelming majority of the properties reproduced by this potential were *not* included in the fitting database. This excellent transferability of the potential was achieved by fitting to *ab initio* formation energies of several real or imaginary compounds with different crystalline structures and chemical compositions across the phase diagram. During the fitting process, the weights of formation energies of different compounds were kept comparable to each other, thus spreading the fitting errors nearly uniformly over the database. This is in contrast to our previous potentials [6,11], which were developed by putting heavy weights on particular properties of either NiAl or Ni_3Al.

Thus, the strategy of giving a high priority to the 'global' fit over insisting on particular properties of particular compounds has payed off by producing a highly transferable, 'universal' potential for the Ni-Al system. This potential is nearly as accurate as the previously developed specialized potentials [6,11] for most of the properties tested in this work. In fact, for a number of properties, the new potential is superior to the specialized potentials [6,11], most notably for phonon frequencies, surface energies and some of the planar fault energies.

One flaw of the new potential is its failure to reproduce the stability of Ni structural vacancies in Al-rich compositions of B2-NiAl. *Ab initio* calculations and experimental measurements, proving or allegedly disproving the existence of such vacancies, have an interesting history that was discussed in [11,46,65] and references therein. Presently, the compositional disorder of NiAl accompanied by the formation of Ni structural vacancies can be taken as an established fact. The criterion of stability of such vacancies is the positive sign and a significant magnitude (0.5–1.0 eV) of the interbranch-Al energy discussed in Section 3.3.

Examination of existing semi-empirical potentials for the Ni-Al system indicates that (i) this criterion is not satisfied by potentials automatically without specifically fitting to it, and (ii) this criterion is only satisfied by the EAM-2002 potential [11] where it was strongly enforced. In the latter case, the fit was achieved at a large expense in accuracy of some other properties. Other potentials give either a negative interbranch-Al energy [6,25,26], or positive but too small to ensure the stability of structural vacancies [24,27].

The difficulty in reproducing the structural vacancies in NiAl is likely to be an intrinsic limitation of the EAM/Finnis–Sinclair formalism. It may have an electronic origin that is yet to be understood. It would be interesting to check if potentials reaching beyond EAM and Finnis–Sinclair framework, for example by including angle-dependent interactions [14,66,67], can reproduce the structural vacancies more easily. In the meantime, the EAM potential developed in this paper can be used for simulations that do not involve the formation of structural vacancies. If they do, then the EAM-2002 potential would present a better choice.

Another advantage of the new potential is that it includes well-established potentials for pure Al [9] and Ni [6]. This makes the potential well suited for simulations of heterophase interfaces or mechanical behavior of two-phase alloys that include the terminal solutions based on either Ni or Al. For example, it can be used for studies of the γ–γ' system as a model of Ni-based superalloys. As another example, we are currently working on certain applications that involve B2-NiAl nano-particles embedded in Al matrix. The new potential should be suitable for simulations of mechanical behavior of such systems.

Acknowledgements

This work was supported by the National Aeronautics and Space Administration through the Langley Research Center (NRA # NNX08AC07A).

Note

1. B2-NiAl melts congruently. Experimental data for the melting point of Ni_3Al vary from 1645 to 1668 K [63]. There is even a controversy about whether this compound melts congruently or via a $\gamma - \gamma'$ eutectic . We use the lower bound of 1645 K.

References

[1] S. Yip, *Handbook of Materials Modeling*, Springer, Dordrecht, The Netherlands, 2005.
[2] J. Hafner, Acta Mater. 48 (2000) p.71.
[3] M.W. Finnis and J.E. Sinclair, Phil. Mag. A 50 (1984) p.45.
[4] M.S. Daw and M.I. Baskes, Phys. Rev. B 29 (1984) p.6443.
[5] M.S. Daw, *Embedded-atom method: Many-body description of metallic cohesion*, in *Atomistic Simulation of Materials: Beyond Pair Potentials*, V. Vitek and D.J. Srolovitz, eds., Plenum Press, New York, 1989, p.181.
[6] Y. Mishin, Acta Mater. 52 (2004) p.1451.
[7] P.L. Williams, Y. Mishin and J.C. Hamilton, Modelling Simul. Mater. Sci. Eng. 14 (2006) p.817.
[8] F. Ercolessi and J.B. Adams, Europhys. Lett. 26 (1994) p.583.
[9] Y. Mishin, D. Farkas, M.J. Mehl and D.A. Papaconstantopoulos, Phys. Rev. B 59 (1999) p.3393.

[10] Y. Mishin, M.J. Mehl, D.A. Papaconstantopoulos, A.F. Voter and J.D. Kress, Phys. Rev. B 63 (2001) p.224106.
[11] Y. Mishin, M.J. Mehl and D.A. Papaconstantopoulos, Phys. Rev. B 65 (2002) p.224114.
[12] R.R. Zope and Y. Mishin, Phys. Rev. B 68 (2003) p.024102.
[13] A. Strachan, T. Cagin, O. Gülseren, S. Mukherjee, R.E. Cohen and W.A. Goddard, Model. Simul. Mater. Sci. Eng 12 (2004) p.S445.
[14] Y. Mishin, M.J. Mehl and D.A. Papaconstantopoulos, Acta Mater. 53 (2005) p.4029.
[15] Y. Mishin and A.Y. Lozovoi, Acta Mater. 54 (2006) p.5013.
[16] H. Chamati, N. Papanicolaou, Y. Mishin and D.A. Papaconstantopoulos, Surf. Sci. 600 (2006) p.1793.
[17] I.J. Robertson, V. Heine and M.C. Payne, Phys. Rev. Lett. 70 (1993) p.1944.
[18] S.L. Frederiksen, K.W. Jacobsen, K.S. Brown and J.P. Sethna, Phys. Rev. Lett. 93 (2004) p.165501.
[19] J. Behler and M. Parrinello, Phys. Rev. Lett. 98 (2007) p.146401.
[20] E. Sanville, A. Bholoa, R. Smith and S.D. Kenny, J. Phys. Condens. Matter 20 (2008) p.285219.
[21] J. Hunger, S. Beyreuther, G. Huttner, K. Allinger, U. Radelof and L. Zsoinal, Euro. J. Inorganic Chem. 6 (1998) p.693.
[22] J.M.C. Marques, F.V. Prudente, F.B. Pereira, M.M. Almeida, A.M. Maniero and C.E. Fellows, J. Phys. B At. Mol. Opt. Phys. 41 (2008) p.085103.
[23] D.W. Brenner, Phys. Status Solidi (b) 217 (2000) p.23.
[24] M. Yan, V. Vitek and S.P. Chen, Acta Metall. Mater. 44 (1996) p.4351.
[25] S.M. Foiles and M.S. Daw, J. Mater. Res. 2 (1987) p.5.
[26] A.F. Voter and S.P. Chen, MRS Symp. Proc. 82 (1987) p.175.
[27] M. Ludwig and P. Gumbsch, Modell. Simul. Mater. Sci. Eng. 3 (1995) p.533.
[28] Y. Mishin, *Interatomic potentials for metals*, in *Handbook of Materials Modeling*, S. Yip, ed., Springer, Dordrecht, The Netherlands, 2005, p.459.
[29] J.R. Rice and J.S. Wang, Mater. Sci. Eng. A 107 (1989) p.23.
[30] V. Vitek, Cryst. Latt. Def. 5 (1974) p.1.
[31] P. Veyssiere and R. Noebe, Phil. Mag. A 65 (1992) p.1.
[32] T. Hong and A.J. Freeman, Phys. Rev. B 43 (1991) p.6446.
[33] C.L. Fu and M.H. Yoo, Acta Metall. Mater. 40 (1992) p.703.
[34] R.D. Noebe, R.R. Bauman and N.V. Nathal, Int. Mater. Rev. 38 (1993) p.34.
[35] M.J. Mills and D.B. Miracle, Acta Metall. Mater. 41 (1993) p.85.
[36] R. Wu, L. Zhong, L. Chen and A.J. Freeman, Phys. Rev. B 54 (1996) p.7084.
[37] A.J. Bradley and A. Taylor, Proc. Roy. Soc. A 159 (1937) p.56.
[38] A. Taylor and N.J. Doyle, J. Appl. Crystallogr. 5 (1972) p.201.
[39] P.A. Korzhavyi, A.V. Ruban, A.Y. Lozovoi, Y.K. Vekilov, I.A. Abrikosov and B. Johansson, Phys. Rev. B 61 (2000) p.6003.
[40] B. Meyer, G. Bester and M. Fähnle, Scripta Mater. 44 (2001) p.2485.
[41] A.Y. Lozovoi, A. Alavi, P.A. Korzhavyi and M.W. Finnis, *Properties of complex inorganic solids*, in *Point Defects in NiAl Under Pressure*, Vol. 2, A. Meike, A. Gonis, P.E.A. Turchi and K. Rajan, eds., Kluwer Academic/Plenum Publishers, New York, 2000.
[42] C.L. Fu, Y.Y. Ye, M.H. Yoo and K.M. Ho, Phys. Rev. B 48 (1993) p.6712.
[43] B. Meyer and M. Fähnle, Phys. Rev. B 59 (1999) p.6072.
[44] Y. Mishin and D. Farkas, Phil. Mag. A 75 (1997) p.169.
[45] Y. Mishin and D. Farkas, Phil. Mag. A 75 (1997) p.187.
[46] A.Y. Lozovoi and Y. Mishin, Phys. Rev. B 68 (2003) p.184113.
[47] C. Stassis, F.X. Kayser, C.K. Loong and D. Arch, Phys. Rev. B 24 (1981) p.3048.
[48] D.P. Pope, *Mechanical properties of intermetallic compounds*, in *Physical Metallurgy*, R.W. Cahn and P. Haasen, eds., Elsevier/North-Holland, Amsterdam, 1996, p.2075.

[49] V. Vitek, D.P. Pope and J.L. Bassani, *Anomalous yield behaviour of compounds with Li_2 structure*, in *Dislocations in Solids*, F.R.N. Nabarro and M.S. Duesbery, eds., Elsevier/North-Holland, Amsterdam, 1996, p.135.
[50] P. Veyssiere and G. Saada, *Microscopy and plasticity of the Li_2 γ' phase*, in *Dislocations in Solids*, F.R.N. Nabarro and M.S. Duesbery, eds., Elsevier/North-Holland, Amsterdam, 1996, p.253.
[51] Y.Q. Sun and P.M. Hazzledine, *Geometry of dislocation glide in Li_2 γ'-phase*, in *Dislocations in Solids*, F.R.N. Nabarro and M.S. Duesbery, eds., Elsevier/North-Holland, Amsterdam, 1996, p.27.
[52] A. Paxton and Y.G. Sun, Phil. Mag. A 78 (1998) p.85.
[53] O.N. Mryasov, Y.N. Gornostyrev, M. van Schilfgaarde and A.J. Freeman, Acta Mater. 50 (2002) p.4545.
[54] G. Schoeck, S. Kohlhammer and M. Fahnle, Phil. Mag. Lett. 79 (1999) p.849.
[55] S. Kohlhammer, M. Fahnle and G. Schoeck, Scripta Mater. 39 (1998) p.359.
[56] K. Hemker and M.J. Mills, Phil. Mag. A 68 (1993) p.305.
[57] H.P. Karnthaler, E.T. Muhlbacher and C. Rentenberger, Acta Mater. 44 (1996) p.547.
[58] T. Kruml, E. Conforto, B.L. Piccolo, D. Caillard and J.L. Martin, Acta Mater. 50 (2002) p.5091.
[59] Y. Mishin and C. Herzig, Acta Mater. 48 (2000) p.589.
[60] J. Sun and T.L. Lin, Acta Metall. Mater. 42 (1994) p.195.
[61] C.L. Fu and G.S. Painter, Acta Mater. 45 (1997) p.481.
[62] T.B. Massalski (ed.), *Binary Alloy Phase Diagrams*, ASM, Materials Park, OH, 1986.
[63] W. Huang and Y.A. Chang, Intermetallics 6 (1998) p.487.
[64] V.A. Ivanov and Y. Mishin, Phys. Rev. B 78 (2008) p.064106.
[65] Y. Mishin, A.Y. Lozovoi and A. Alavi, Phys. Rev. B 67 (2003) p.014201.
[66] M.I. Baskes, Phys. Rev. Lett. 59 (1987) p.2666.
[67] M.I. Baskes, Phys. Rev. B 46 (1992) p.2727.
[68] C. Kittel, *Introduction to Sold State Physics*, Wiley-Interscience, New York, 1986.
[69] R. Hultgren, P.D. Desai, D.T. Hawkins, M. Gleiser and K.K. Kelley (eds.), *Selected Values of the Thermodynamics Properties of Binary Alloys*, ASM, Metals Park, OH, 1973.
[70] N. Rusovic and H. Warlimont, Phys. Status Solidi A 44 (1977) p.609.
[71] N.I. Medvedeva, O.N. Mryasov, Y.N. Gornostyrev, D.L. Novikov and A.J. Freeman, Phys. Rev. B 54 (1996) p.13506.
[72] M.H. Yoo and C.L. Fu, Scr. Metall. Mater. 25 (1991) p.2345.
[73] A.T. Hanbicki, A.P. Baddorf, E.W. Plummer, B. Hammer and M. Scheffler, Surf. Sci. 331–333 (1995) p.811.
[74] M.H. Yoo, Acta Metall. 35 (1987) p.1559.
[75] M.H. Yoo, M.S. Daw and M.I. Baskes, *Atomistic simulation of superdislocation dissociation in Ni_3Al*, in *Atomistic Simulation of Materials: Beyond Pair Potentials*, V. Vitek and D.J. Srolovitz, eds., Plenum Press, New York, 1989, p.401.
[76] R.C. Weast (ed.), *Handbook of Chemistry and Physics*, CRC, Boca Raton, FL, 1984.
[77] F.X. Kayser and C. Stassis, Phys. Status Solidi (a) 64 (1981) p.335.
[78] R. Hultgren, P.D. Desai, D.T. Hawkins, M. Gleiser and K.K. Kelley (eds.), *Selected Values of the Thermodynamics Properties of Binary Alloys*, ASM, Metals Park, OH, 1973.
[79] M. Ellner, S. Kek and B. Predel, J. Less Comm. Metals 154 (1989) p.207.
[80] E.A. Brandes (ed.), *Smithells Metals Reference Book*, Vol. 6, Butterworths, London, 1983.
[81] M. Mostoller, R.M. Nicklow, D.M. Zehner, S.C. Lui, J.M. Mundenar and E.W. Plummer, Phys. Rev. B 40 (1989) p.2856.
[82] Y.S. Touloukian, R.K. Kirby, R.E. Taylor and P.D. Desai (eds.), *Thermal Expansion: Metallic Elements and Alloys*, Vol. 12, Plenum, New York, 1975.